How Optical and Electrical Properties of ITO Coated Willow Glass Affect Photonic Curing Outcome for Upscaling Perovskite Solar Cell Manufacturing

Robert T. Piper, Weijie Xu, and Julia W. P. Hsu

***Abstract*—Indium tin oxide (ITO) coated Willow® glass is an excellent substrate for roll-to-roll manufacturing of perovskite solar cells (PSCs) but can have large variability in its optical and electrical properties. Photonic curing uses intense light pulses instead of heat to process materials and can facilitate faster processing speeds in roll-to-roll manufacturing to upscale the production of PSCs. Since the entire film stack can absorb light and contributes to the photonic curing outcome, the substrate materials' properties play an integral role. Here, we present the effect of ITO transmittance on the photonic curing of nickel nitrate sol-gel precursors into nickel oxide and consequently the performance of PSCs fabricated with only photonic curing and no thermal annealing. Unexpectedly, ITO samples processed by photonic curing show improved optical and electrical properties.**

***Index Terms*—high throughput, perovskite solar cells, photonic curing**

I. Introduction

PEROVSKITE solar cells (PSCs) have shown significant progress compared to other photovoltaic technologies, with efficiencies reaching 17.9% for module sizes between 800 – 6,500 cm^2 [1]. Halide perovskites have the advantage of solution processibility with excellent optoelectronic properties. Using a single roll-to-roll production line with a 1.5 m web width at 30 m/min web speed, a yield of up to 4 GW/year is forecast [2]. To drive down the cost of PSC manufacturing, improvements must be made towards higher throughput by increasing the processing speed and device area [3]. Thermal annealing requires large-size annealing tools and a slow web speed due to the long time required (tens of minutes). One promising approach to meet these goals is adapting photonic curing, also known as intense pulsed light annealing, instead of thermal annealing for materials processing.

Photonic curing uses short (microsecond to millisecond) pulses of broadband light (200 – 1500 nm) from a xenon flash lamp to deliver low energy (< 100 J/cm^2) but high power (up to 50 kW/cm^2) to the sample. The light pulses are absorbed by any light-absorbing component in the sample, upon which the radiant energy is converted to heat to drive the transformation (oxide calcination, crystallization, phase change, etc.) of the materials being processed. Photonic curing has been applied to several materials in PSCs: halide perovskite active layers [4]–[9], NiO_x sol-gel hole transport layer (HTL) [4], SnO_2 nanoparticle and sol-gel electron transport layer (ETL) [9], [10], and mesoporous and compact TiO_2 ETL [11]–[13]. In addition, photonic curing has been used to anneal sputtered indium tin oxide (ITO) films on Corning Willow® (WG) glass and achieve similar optical and electrical properties as thermally annealed ITO films, but with a much shorter time [14]. Photonic curing takes milliseconds, thereby increasing roll-to-roll web speed by orders of magnitude [4]–[7].

For transparent films that are not strongly light-absorbing, e.g., wide-bandgap metal oxides, light-absorbing materials can aid the processing outcome of the films when using photonic curing. Daunis et al. [15] demonstrated that ZrO_2 films on Al pads can be converted at a lower radiant energy than on the bare polyethylene naphthalate substrate. Conducting oxide (e.g., ITO) or metal (e.g., Al) layers on the transparent substrate act as the light-absorbing materials that generate heat to convert the non-light-absorbing sol-gel precursors into metal oxide films. We previously applied photonic curing to process NiO_x HTL and methylammonium lead iodide ($MAPbI_3$) active layers and achieved a power conversion efficiency (PCE) of 12% with *p-i-n* PSCs on WG/ITO without any thermal annealing [4]. WG/ITO is an excellent substrate candidate for flexible PSCs because of its compatibility with large area, roll-to-roll manufacturing. Interestingly, we noticed that the optical transmittance of WG/ITO sheets varies greatly. We find that the optical transmittance of the WG/ITO determines the extent of NiO_x conversion during photonic curing and has a large impact on PSC performance. Here we report a detailed study on the variation of optical transmittance and sheet resistance for a variety of ITO (~150 nm) coated WG (100 μm, Fraunhofer FEP) substrates and how their properties affect the performance of PSCs made with photonic cured NiO_x HTLs and photonic cured $MAPbI_3$ active layers without any thermal annealing.

This manuscript is an enhanced version of [16], published in the 2021 IEEE photovoltaic specialists conference proceedings.

This work is funded in part by the U.S. Department of Energy Solar Energy Technologies Office under Award Numbers DE-EE0008544 and DE-EE0009518 (Corresponding author: J.W.P.H.). R.T.P. acknowledges support from NSF CBET-1916612. J.W.P.H. acknowledges support from the Texas Instruments Distinguished Chair in Nanoelectronics.

R.T.P. (Robert.piper@utdallas.edu), W.X. (Weijiexu@utdallas.edu), and J.W.P.H. (jwhsu@utdallas.edu) are with the University of Texas at Dallas, Richardson, TX, 75080 USA.

The following enhancements have been made to the manuscript. Optical transmittance, sheet resistance, and light absorption data for additional WG/ITO samples have been added to Fig. 1, including sheet resistance and transmittance measurements before and after processing via thermal annealing or photonic curing. Champion *J-V* data in Fig. 2, including adding data for dark WG/ITO substrates, have been updated with more recent results. XPS analysis of photonic cured NiO_x films and SimPulse® simulations for dark WG/ITO substrates were added to Fig. 3. New *J-V* data for solar cell devices made with NiO_x photonic cured by a single light pulse have been added as Fig. 4. An experimental section has been added to include specific information on device fabrication and materials characterization.

II. Materials and Methods

A. Device Fabrication

The PSC device structure is, listed from bottom to top, WG/ITO/NiO_x/$MAPbI_3$/Phenyl-C_{61}-butyric acid methyl ester (PCBM)/bathocuproine (BCP)/Al. The WG/ITO substrates were rinsed with DI water and blown dry with N_2 before being UV-ozone treated (Bioforce Nanosciences Procleaner Plus) for 20 min. All chemicals were purchased from Acros Organics or Sigma-Aldrich, unless otherwise specified. NiO_x precursor solution was made, modified from [17], by first dissolving 0.1 M nickel nitrate hexahydrate in 2-methoxyethanol. Then, 0.1 M acetylacetone was added and the solution was stirred overnight at room temperature. The NiO_x precursor solution (clear emerald green color) was filtered (0.2 μm polytetrafluoroethylene filter) before spin coating at 3,000 rpm for 30 s. The spin coated wet films were then dried on a hot plate at 70°C for 3 min and then converted to NiO_x via thermal annealing or photonic curing. Both processes are done in open air at ambient conditions (30-50% relative humidity). The thermal annealing process was performed on dried precursor films on a hot plate at 250°C for 30 min. Two different photonic curing processes were used to convert the NiO_x film from nickel nitrate precursor solution: a ten-pulse process at low voltage and a one-pulse process at high voltage. A NovaCentrix PulseForge® Invent with one 500 V lamp driver and a 1.5 kW power supply was used for the ten-pulse photonic curing process, with the following parameters: 500 V lamp voltage, 3.5 ms pulse length, 10.5 J/cm^2 pulse fluence and a repetition rate of 0.35 Hz. A PulseForge® Invent equipped with two 950 V lamp drivers and a 1.5 kW power supply was used for the one-pulse photonic curing process, with the following parameters: 790 V lamp voltage, 1.1 ms pulse length, and 12.7 J/cm^2 pulse fluence. Both photonic curing tools have a 20 mm diameter lamp that is 150 mm long, producing a uniform illumination area of 150 mm by 75 mm. The NiO_x film was determined to be ~30 nm using spectroscopic ellipsometry.

$MAPbI_3$ precursor solution (1.4 M) was made, modified from [18], by dissolving lead (II) iodide (TCI America, 99.99%), methylammonium iodide (GreatCell Solar), and dimethyl sulfoxide (equal molar ratio) in N,N-dimethylformamide. Diiodomethane (175 μL) was added to the $MAPbI_3$ precursor solution to enhance the device performance [19], [20]. The final $MAPbI_3$ concentration with diiodomethane added is 1.1 M. The solution was stirred for at least two hours before filtering (0.2 μm polytetrafluoroethylene filter) then spin coating at 4,000 rpm for 25 s inside an N_2-purged glovebox. One mL of diethyl ether was dispensed onto the sample after 10 s of spinning. All $MAPbI_3$ films were photonic cured in ambient, open air conditions with the 500-V PulseForge® Invent immediately after spin coating using one pulse at 290 V lamp voltage and 20 ms pulse length. After photonic curing the $MAPbI_3$ layer, the samples were returned to the N_2-purged glovebox to deposit the ETLs. The $MAPbI_3$ film was determined to be ~300 nm using spectroscopic ellipsometry. PCBM (Lumtec) in chlorobenzene (20 mg/mL) was spin coated at 1,200 rpm for 60 s followed by spin coating BCP in anhydrous ethanol (0.5 mg/mL) at 4,000 rpm for 30 s. No annealing step was performed on either ETL. The top contact was 100 nm of Al thermally evaporated through a shadow mask to form 6 diodes with a 0.11 cm^2 area.

B. Device and Materials Characterization

UV-vis absorption and transmittance were measured using an Ocean Optics 4000 USB spectrometer in transmission mode. Sheet resistance was measured with an Alessi four-point probe consisting of four electrical contacts in a line. Current density-voltage (*J-V*) measurements were collected with an AM 1.5G 100 mW/cm^2 AAA solar simulator (Abet) and a 2635A Keithley source-meter. Voltage was ramped from -0.2 to 1.2 V for forward scans and 1.2 to -0.2 V for reverse scans under illumination. The aperture area was 0.049 cm^2 and the voltage scan rate was 70 mV/s. *J-V* measurements were performed inside of an N_2-filled glovebox. XPS was performed on an Ulvac-PHI VersaProbe2 with a monochromated Al Ka source (1486.8 eV) at a 45° angle to the sample surface at 50W and 15 kV with a 200 μm beam size. Ni $2p_{3/2}$ spectra were averaged over 20 scans with an energy step of 0.1 eV at 20 ms per step and a pass energy of 23.5 eV. N 1s spectra were averaged over five scans with an energy step of 0.8 eV at 20 ms per step and a pass energy of 187.85 eV. XPS fitting was done using MultiPak software (Ulvac-PHI) following the same method as [4]. The N 1s peak area was calculated between 401 and 413 eV. The Ni $2p_{3/2}$ spectra were fitted with seven peaks with peak 1 at the lowest binding energy (BE) and peak 7 at the highest BE. Peak 1 through peak 4 are used to fit the primary Ni $2p_{3/2}$ peaks, and peak 5 through peak 7 are used to fit the higher BE satellite peaks. Variable angle spectroscopic ellipsometry measurements were done using an J.A. Woolam M-2000DI at incident angles of 55°, 65°, and 75°. The incident light wavelength ranges from 192 to 1690 nm. Index of refraction, extinction coefficient, and thickness for WG and ITO were determined from CompleteEase software by fitting the ellipsometry data using a Cauchy model for the uncoated WG substrate and a general oscillator model for the WG/ITO substrates.

III. Results and Discussion

Fig. 1a shows representative UV-vis spectra (referenced to air) for WG/ITO we classify as light, medium, and dark categories. T_{avg} is the average transmittance through the WG/ITO substrates from 400 to 800 nm wavelengths. Spectroscopic ellipsometry results for the WG/ITO reveal non-uniformity in the optical constants as a function of depth into the ITO layer. To achieve a good fit to the ellipsometry data, the ITO on WG must be modeled as five layers with distinct indices of refraction and extinction coefficients for each layer [4]. The overall ITO layer thickness from ellipsometry is 141 nm, 140 nm, and 146 nm for light, medium, and dark WG/ITO substrates, respectively. Therefore, the optical differences between the substrates are not due to thickness variations.

Fig. 1b shows that the sheet resistance (R_{sh}, left axis) decreases as T_{avg} of the WG/ITO increases. The light absorption (right axis) of the WG/ITO substrates are determined by using a calibrated bolometer to measure the radiant energy of pulsed light passing through the sample and referencing to the full radiant energy without a sample, as described in [4]. As T_{avg} increases, the absorption of light from the xenon flash lamp by the sample reduces. Ten WG/ITO substrates with varying T_{avg} (circled in Fig. 1b) were selected and subjected to either thermal annealing (cyan, 250°C 30 min) or photonic curing (orange, 500 V 3.5 ms 10 pulses 0.35 Hz) processes without any NiO_x film to probe the effects of processing on the ITO alone. T_{avg} and R_{sh} were measured before (striped bars) and after (solid bars) processing. Fig. 1c shows that the T_{avg} increases after both thermal annealing and photonic curing processes. Dark WG/ITO substrates have the highest (~10%) increase in T_{avg} after both processes. The increase in T_{avg} due to processing decreases with increasing sample transmittance and becomes negligible for light WG/ITO. We speculate that the darker samples have an ITO layer that is not fully converted in the manufacturing process. This is further evidenced by the higher R_{sh} measured on the darker WG/ITO substrates as shown in Fig. 1b. Unexpectedly, Fig. 1d shows that thermal annealing and photonic curing have opposite effects on WG/ITO R_{sh} independent of the initial WG/ITO transmittance: the ITO R_{sh} increases after thermal annealing whereas it decreases after photonic curing. Dark WG/ITO substrates have ~6% ***higher*** R_{sh} after thermal annealing and ~28% ***lower*** R_{sh} after photonic curing. Because light WG/ITO substrates are affected less by the photonic curing process than darker ones, the improvement in their R_{sh} is smaller (~3%). Therefore, the photonic curing process has an additional advantage over thermal annealing when processing materials on top of WG/ITO substrates in that both the electrical and optical properties of the ITO are improved after the photonic curing.

For PSCs with thermal annealed NiO_x HTLs, ITO films with high transmittance are desirable to maximize the light intensity reaching the perovskite absorber layer. PSCs with thermally annealed NiO_x HTLs show a decrease in J_{SC} as the WG/ITO substrate becomes darker, with PSCs made on light WG/ITO substrates yielding the highest J_{SC}. Furthermore, thermal annealed PSCs made on light and medium WG/ITO give similar PCE (9.9% ± 0.9%), whereas dark WG/ITO samples have ~30% reduced PCE (6.9% ± 0.7%). The PCE reduction for dark WG/ITO substrates in thermal annealed samples is attributed to the lower transmittance and higher sheet resistance of the dark WG/ITO after thermal annealing (Fig. 1c and 1d).

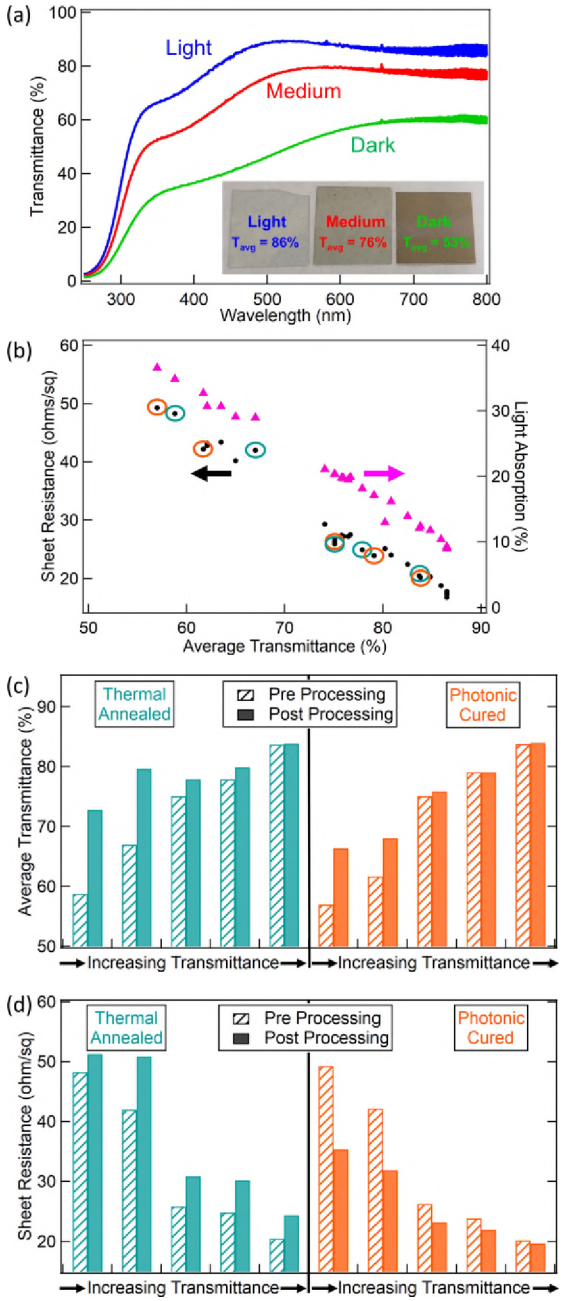

Fig. 1 (a) UV-vis transmittance of light (blue), medium (red), and dark (green) WG/ITO substrates. The inset shows an image of the three types of WG/ITO with their average transmittance from 400 to 800 nm. (b) Sheet resistance (black circles, left) and light absorption measured using a calibrated bolometer (magenta triangles, right) versus average transmittance. Ten WG/ITO samples were chosen for processing via thermal annealing (cyan circles) or photonic curing (orange circles). (c) Average transmittance of WG/ITO circled in (b) pre (striped) and post (solid) thermal annealing (cyan, left) or photonic curing (orange, right). (d) Sheet resistance of the same WG/ITO as (c) pre and post thermal annealing or photonic curing. The average transmittance increases from left to right for each process in (c) and (d).

However, this trend does not apply to photonic cured samples, as the mechanisms are different. Processing with photonic curing requires a light-absorbing layer to convert the energy of the incoming photons into heat because NiO_x sol-gel

precursor is mostly transparent and very thin (~ 30 nm), hence not able to absorb enough light to effectively convert to metal oxide on its own. Bolometry measurements show that the WG/ITO absorbs between 9 to 38% of the incoming light (Fig. 1b right axis). Therefore, ITO layers with different transmittance absorb different amounts of light and generate different amounts of heat to convert NiO_x sol-gel precursor. Fig. 2a shows the champion *J-V* plot for *p-i-n* photonically cured PSCs made on light (T_{avg} = 88%), medium (T_{avg} = 71%), and dark (T_{avg} = 60%) WG/ITO substrates. Both NiO_x HTLs and $MAPbI_3$ absorber layers were photonic cured, i.e., no thermal annealing was used to fabricate these devices. While one might expect devices made on light WG/ITO to perform the best because more light can reach the perovskite absorber layer, our results show that devices made on the medium WG/ITO substrate have significantly better PSC performance than on the light and dark WG/ITO, with champion V_{OC} = 0.948 V, J_{SC} = 14.2 mA/cm^2, FF = 75%, and PCE = 10.1%. In contrast, devices made on the light WG/ITO substrate have champion V_{OC} = 0.857 V, J_{SC} = 2.04 mA/cm^2, FF = 19% and PCE = 0.33%. However, using a WG/ITO substrate that is too dark can be detrimental to device performance. Devices made on the dark WG/ITO have champion V_{OC} = 0.969 V, J_{SC} = 12.65 mA/cm^2, FF = 55% and PCE = 6.7%. Compared to medium WG/ITO substrates there is a reduction in J_{SC} and FF, leading to a reduction in PCE, on the dark WG/ITO substrates. Similar to the thermal annealed results, the reduction in J_{SC} and FF are attributed to the lower transmittance and higher sheet resistance, respectively, of the dark WG/ITO. These results show that the transmittance of the substrate plays a large role in determining device performance when using photonic curing for materials processing. These results are robust from run to run. Box plots of the reverse scan *J-V* data are presented in Fig. 2b. Thus, there is a tradeoff between high transmittance for solar cell performance and light absorption required for photonic curing to be effective.

We hypothesize that the optical transmittance of the substrates affects the NiO_x photonic curing outcome which directly affects the device results in Fig. 2 and perform XPS to evaluate the degree of conversion to NiO_x on different WG/ITO substrates. Fig. 3a shows fitted XPS Ni $2p_{3/2}$ spectra for photonic cured NiO_x films deposited on light (T_{avg} = 86%), medium (T_{avg} = 76%), and dark (T_{avg} = 53%) WG/ITO. The Ni $2p_{3/2}$ and N 1s signals for the same samples are summarized in Fig. 3b. As described in [4], Ni $2p_{3/2}$ peak 1, at a BE of ~854 eV, (Fig. 3a blue areas, Fig. 3b solid bars) is attributed to Ni in the NiO chemical state [21] and Ni $2p_{3/2}$ peak 2, at a BE of ~855 eV, (Fig. 3a orange areas, Fig. 3b striped bars) is attributed to various Ni hydroxide species, including α and β-$Ni(OH)_2$ and NiOOH with Ni in the 2+ and 3+ oxidation states [22]–[24]. The N 1s peak (Fig. 3b black circles) is associated with the presence of nitrate in the sample from the nickel nitrate precursor and indicates an unconverted or partially converted sample [27]. The NiO_x film made on the light WG/ITO is not fully converted from precursor, as evidenced by the absence of Ni $2p_{3/2}$ peak 1 and high Ni $2p_{3/2}$ peak 2 signals. In addition, there is a large N 1s peak in the light WG/ITO sample. The XPS spectra of the photonic cured NiO_x on light WG/ITO are similar to those of dried nickel nitrate sol-gel precursor film [4].

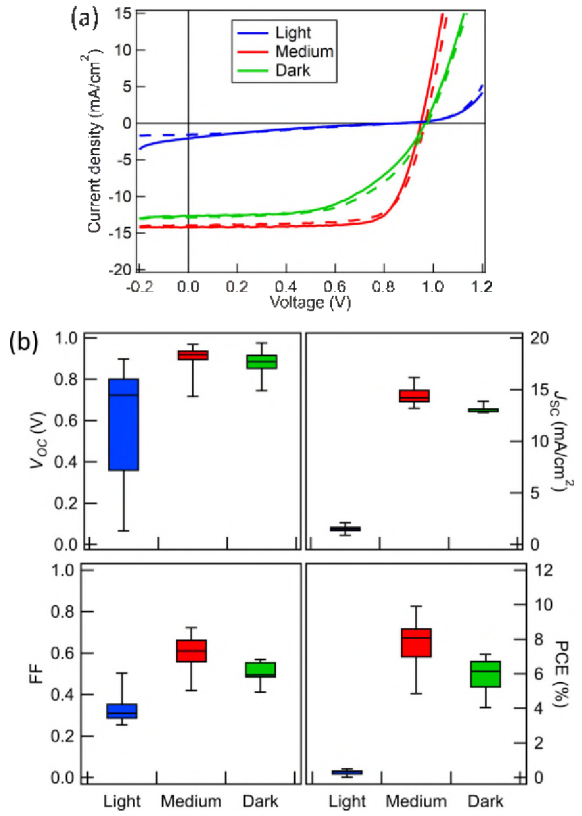

Fig. 2 (a) Champion *J-V* curves for photonically cured PSCs made on light (blue), medium (red), and dark (green) WG/ITO substrates. Solid lines and dashed lines represent forward and reverse scan directions, respectively. (b) Box plots of the reverse scan direction *J-V* parameters V_{OC}, J_{SC}, FF, and PCE for PSCs made on light (blue, 15 diodes), medium (red, 29 diodes), and dark (green, 9 diodes) WG/ITO substrates. The box plots show the first quartile, median, and third quartile. The whiskers represent minimum and maximum values.

In contrast, the NiO_x film made on medium and dark WG/ITO substrates show a higher degree of conversion with increased Ni $2p_{3/2}$ peak 1 area and reduced Ni $2p_{3/2}$ peak 2 area. Furthermore, there is no N 1s peak, indicating that all the nitrates have been removed as the nickel nitrate becomes converted into NiO_x. These XPS spectra are similar to those of thermal annealed NiO_x films [4]. Fig. 3c compares the UV-vis absorbance of photonic cured NiO_x films on light and medium WG/ITO. The NiO_x film processed on the medium WG/ITO shows a much larger absorbance peak (OD ~ 0.15) at 300 nm than that on the light WG/ITO substrate (OD = 0.03), confirming the XPS results that the NiO_x is converted on the medium WG/ITO but not on the light WG/ITO.

To understand these observations, we perform SimPulse® simulations to obtain temperature versus time profiles during photonic curing for light (10% light absorption), medium (25% light absorption), and dark (34% light absorption) WG/ITO (Fig. 3d). The light absorption values used are the same as the values measured via bolometry on the substrates used for the device results in Fig. 2a. The simulation results show that the maximum temperature reached is 188°C, 410°C, and 535°C for light, medium and dark WG/ITO substrates, respectively. This large difference in the processing temperature explains the NiO_x photonic curing outcome shown in Fig. 2. Because the light absorption of the light WG/ITO is low, the nickel nitrate

sol-gel precursor is not completely converted to NiO_x by photonic curing. The medium and dark WG/ITO absorb more photons and reach higher temperatures, enabling the NiO_x sol-gel precursor to convert to metal oxide. Typically, thermal processing on ITO is conducted at temperatures below ~300°C to avoid degradation of the ITO's electrical properties. Photonic curing, however, delivers much lower total energy than hot plate or furnace annealing because of the much shorter processing time. Although the ITO layer can reach temperatures above 500°C during photonic curing on darker samples, it is only at high temperature for milliseconds and no loss of electrical conductivity or mechanical strength is observed. In fact, we show an improvement in the ITO electrical conductivity after photonic curing (Fig. 1d).

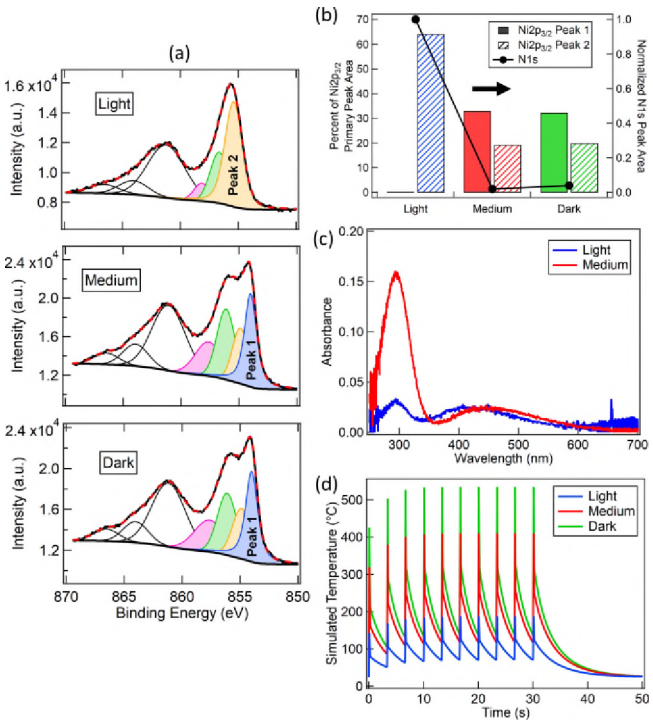

Fig. 3 (a) XPS Ni $2p_{3/2}$ spectra with fitted curves of photonic cured NiO_x on light (top), medium (middle), and dark (bottom) WG/ITO. Peak 1 and 2 are represented by the blue and orange fitting curves, respectively. (b) Percent of Ni $2p_{3/2}$ peak 1 (solid bars) and peak 2 (striped bars) in the total primary peak area for the XPS spectra shown in (a) (left) and normalized N 1s peak area (black dots, right). (c) UV-vis absorbance for NiO_x films photonic cured on light (blue) and medium (red) WG/ITO. (d) SimPulse® simulated surface temperature of light (blue), medium (red), and dark (green) WG/ITO undergoing the ten-pulse photonic curing process.

To reach high-throughput manufacturing using a roll-to-roll process with photonic curing, it is advantageous to reduce the processing time as much as possible. To achieve this, we use a more powerful PulseForge® Invent to photonic cure the NiO_x in a single pulse. Fig. 4a shows champion PSC results for NiO_x made by the one-pulse NiO_x photonic curing process (purple) compared to the ten-pulse photonic curing process (red). Fig. 4b shows box plots of the reverse scan device parameters. Both processes were done using medium WG/ITO substrates (T_{avg} = 71 – 77%). These results show that the one-pulse process reduces the hysteresis and outperforms the ten-pulse process with a higher average V_{OC}, J_{SC}, and PCE. For the ten-pulse process, the lamp drivers must be recharged by a power supply between each pulse. The power output of the power supply will determine how fast this recharging occurs, i.e., time between multiple pulses, which directly affect the web speed. The overall processing time for these photonic curing conditions are 26 s for the ten-pulse process versus 1.1 ms for the one-pulse process. Therefore, the processing time is reduced by four orders-of-magnitude using one pulse compared to ten pulses and six orders-of magnitude compared to 30 min of thermal annealing.

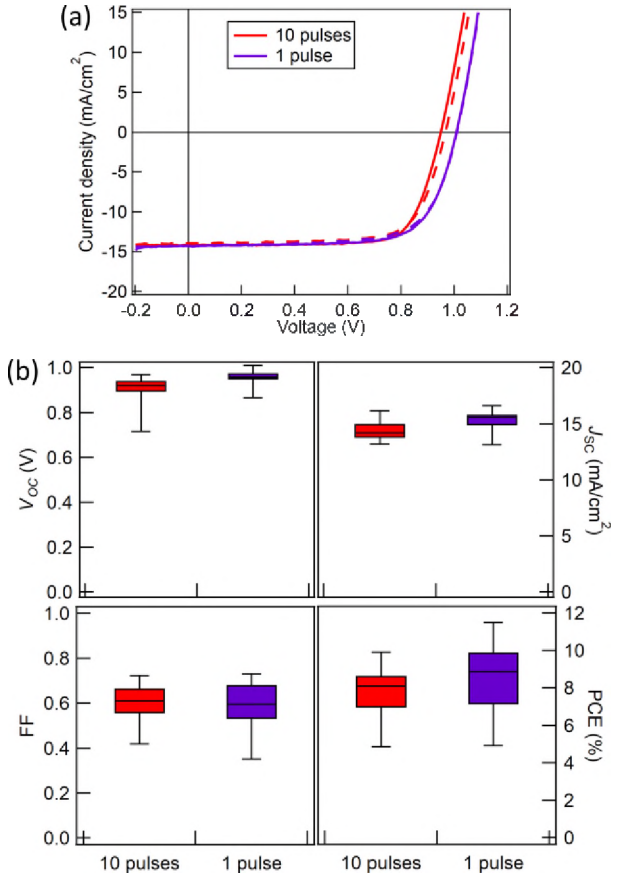

Fig. 4 (a) Champion *J-V* curves for PSCs made on medium WG/ITO where NiO_x was converted with the ten-pulse (red) or the one-pulse (purple) photonic curing process. Solid lines and dashed lines represent forward and reverse scan directions, respectively. (b) Box plots of the reverse scan direction *J-V* parameters V_{OC}, J_{SC}, FF, and PCE for PSCs made with NiO_x photonic cured with the ten-pulse (red, 29 diodes) or the one-pulse (purple, 30 diodes) process. The box plots show the first quartile, median, and third quartile. The whiskers represent minimum and maximum values.

IV. Summary

We find that the variability in WG/ITO optical transmittance can lead to drastically different PSC performance (Fig. 2a) when photonic curing is used to convert the NiO_x HTL. There is an optimal point in substrate optical transmittance where the light absorption is high enough to enable conversion of NiO_x sol-gel precursor without reducing the amount of light that reaches the $MAPbI_3$ absorber layer too much. Therefore, the light absorption and optical transmittance of the substrate and conducting oxide are important considerations when fabricating PSCs using photonic curing. As photonic curing improves ITO properties (Fig. 1c and 1d), it may be possible to simultaneously

convert NiO_x HTLs and improve ITO performance, enabling higher J_{SC} values. To achieve large area, roll-to-roll manufacturing using photonic curing, it is critical to have tight control of the substrate quality (i.e., low variability in optical transmittance and light absorption) to have a consistent process. Any variations in these properties will have a large impact on photonic curing, particularly when the ITO layer is the primary light-absorbing component in the sample stack. Here we demonstrate that high transmittance WG/ITO do not absorb enough light in the photonic curing process to convert NiO_x sol-gel precursor into metal oxide. In contrast, medium and dark WG/ITO could be used to process NiO_x metal oxide films with photonic curing to fabricate functional PSCs. Furthermore, the medium and dark WG/ITO showed a reduction in sheet resistance and an enhancement in optical transmittance after photonic curing. To optimize photonic curing for processing a particular material system, it is important to consider the optical properties of the substrate materials as this can dramatically affect the photonic curing process parameters and the manufacturing yield.

ACKNOWLEDGMENT

We thank Energy Materials Corporation for providing the WG/ITO and R. Wallace for use of spectroscopic ellipsometer.

DISCLAIMER

This report was prepared as an account of work sponsored by an agency of the United States Government. Neither the United States Government nor any agency thereof, nor any of their employees, makes any warranty, express or implied, or assumes any legal liability or responsibility for the accuracy, completeness, or usefulness of any information, apparatus, product, or process disclosed, or represents that its use would not infringe privately owned rights. Reference herein to any specific commercial product, process, or service by trade name, trademark, manufacturer, or otherwise does not necessarily constitute or imply its endorsement, recommendation, or favoring by the United States Government or any agency thereof. The views and opinions of authors expressed herein do not necessarily state or reflect those of the United States Government

REFERENCES

[1] National Renewable Energy Laboratory (NREL), "Champion Photovoltaic Module Efficiency Chart," *Nrel*, 2020. https://www.nrel.gov/pv/module-efficiency.html (accessed Apr. 16, 2021).

[2] EMC, "High Speed Inline Roll-to-Roll Module Production," 2020. https://enmatcorp.com/high-speed-inline-roll-to-roll-module-production/ (accessed Nov. 15, 2020).

[3] B. Martin, D. Amos, E. Brehob, M. F. A. M. van Hest, and T. Druffel, "Techno-economic analysis of roll-to-roll production of perovskite modules using radiation thermal processes," *Appl. Energy*, no. October, p. 118200, 2021, doi: 10.1016/j.apenergy.2021.118200.

[4] R. T. Piper, T. B. Daunis, W. Xu, K. A. Schroder, and J. W. P. Hsu, "Photonic Curing of Nickel Oxide Transport Layer and Perovskite Active Layer for Flexible Perovskite Solar Cells: A Path Towards High-Throughput Manufacturing," *Front. Energy Res.*, vol. 9, p. 76, 2021, doi: 10.3389/fenrg.2021.640960.

[5] W. Xu, T. B. Daunis, R. T. Piper, and J. W. P. Hsu, "Effects of Photonic Curing Processing Conditions on MAPbI3Film Properties and Solar Cell Performance," *ACS Appl. Energy Mater.*, vol. 3, no. 9, pp. 8636–8645, 2020, doi: 10.1021/acsaem.0c01243.

[6] A. H. Ghahremani, S. Pishgar, J. Bahadur, and T. Druffel, "Intense Pulse Light Annealing of Perovskite Photovoltaics Using Gradient Flashes," *ACS Appl. Energy Mater.*, vol. 3, no. 12, pp. 11641–11654, 2020, doi: 10.1021/acsaem.0c01520.

[7] J. Troughton *et al.*, "Photonic flash-annealing of lead halide perovskite solar cells in 1 ms," *J. Mater. Chem. A*, vol. 4, no. 9, pp. 3471–3476, 2016, doi: 10.1039/c5ta09431c.

[8] B. W. Lavery, S. Kumari, H. Konermann, G. L. Draper, J. Spurgeon, and T. Druffel, "Intense Pulsed Light Sintering of CH3NH3PbI3 Solar Cells," *ACS Appl. Mater. Interfaces*, vol. 8, no. 13, pp. 8419–8426, 2016, doi: 10.1021/acsami.5b10166.

[9] A. H. Ghahremani, B. Martin, A. Gupta, J. Bahadur, K. Ankireddy, and T. Druffel, "Rapid fabrication of perovskite solar cells through intense pulse light annealing of SnO2 and triple cation perovskite thin films," *Mater. Des.*, vol. 185, p. 108237, Jan. 2020, doi: 10.1016/j.matdes.2019.108237.

[10] M. Zhu *et al.*, "Millisecond-pulsed photonically-annealed tin oxide electron transport layers for efficient perovskite solar cells," *J. Mater. Chem. A*, vol. 5, no. 46, pp. 24110–24115, 2017, doi: 10.1039/c7ta07969a.

[11] S. Das *et al.*, "Low thermal budget, photonic-cured compact TiO2 layers for high-efficiency perovskite solar cells," *J. Mater. Chem. A*, vol. 4, no. 24, pp. 9685–9690, 2016, doi: 10.1039/c6ta02105k.

[12] B. Feleki, G. Bex, R. Andriessen, Y. Galagan, and F. Di Giacomo, "Rapid and low temperature processing of mesoporous TiO2 for perovskite solar cells on flexible and rigid substrates," *Mater. Today Commun.*, vol. 13, pp. 232–240, Dec. 2017, doi: 10.1016/j.mtcomm.2017.09.007.

[13] S. Luo *et al.*, "Instantaneous photoinitiated synthesis and rapid pulsed photothermal treatment of three-dimensional nanostructured TiO2 thin films through pulsed light irradiation," *J. Mater. Res.*, vol. 32, no. 9, pp. 1701–1709, May 2017, doi: 10.1557/jmr.2017.139.

[14] M. Junghähnel, S. Weller, and T. Gebel, "P-65: Advanced Processing of ITO and IZO Thin Films on Flexible Glass," in *SID Symposium Digest of Technical Papers*, Jun. 2015, vol. 46, no. 1, pp. 1378–1381, doi: 10.1002/sdtp.10131.

[15] T. B. Daunis, K. A. Schroder, and J. W. P. Hsu, "Photonic curing of solution-deposited ZrO2 dielectric on PEN: a path towards high-throughput processing of oxide electronics," *npj Flex. Electron.*, vol. 4, no. 1, p. 7, Dec. 2020, doi: 10.1038/s41528-020-0070-4.

[16] R. T. Piper, W. Xu, and J. W. P. Hsu, "Optical and Electrical Properties of ITO Coated Willow Glass for Upscaling Perovskite Solar Cell Manufacturing Using Photonic Curing," *Conf. Rec. IEEE Photovolt. Spec. Conf.*, pp. 2293–2295, 2021, doi: 10.1109/PVSC43889.2021.9518965.

[17] Z. Liu *et al.*, "High-Performance Planar Perovskite Solar Cells Using Low Temperature, Solution–Combustion-Based Nickel Oxide Hole Transporting Layer with Efficiency Exceeding 20%," *Adv. Energy Mater.*, vol. 8, no. 19, pp. 1–9, 2018, doi: 10.1002/aenm.201703432.

[18] N. Ahn, D. Y. Son, I. H. Jang, S. M. Kang, M. Choi, and N. G. Park, "Highly Reproducible Perovskite Solar Cells with Average Efficiency of 18.3% and Best Efficiency of 19.7% Fabricated via Lewis Base Adduct of Lead(II) Iodide," *J. Am. Chem. Soc.*, vol. 137, no. 27, pp. 8696–8699, Jul. 2015, doi: 10.1021/jacs.5b04930.

[19] W. Xu, R. T. Piper, and J. W. P. Hsu, "CH2I2 improves photocurrent and supress ionic motion in photonically cured MAPbI3 solar cells."

[20] K. Ankireddy, A. H. Ghahremani, B. Martin, G. Gupta, and T. Druffel, "Rapid thermal annealing of CH3NH3PbI3 perovskite thin films by intense pulsed light with aid of diiodomethane additive," *J. Mater. Chem. A*, vol. 6, no. 20, pp. 9378–9383, 2018, doi: 10.1039/c8ta01237g.

[21] A. N. Mansour, "Characterization of NiO by XPS," *Surf. Sci. Spectra*, vol. 3, no. 3, pp. 231–238, 1994, doi: 10.1116/1.1247751.

[22] A. N. Mansour and C. A. Melendres, " Characterization of α-Ni(OH) 2 by XPS ," *Surf. Sci. Spectra*, vol. 3, no. 3, pp. 255–262, Jul. 1994, doi: 10.1116/1.1247754.

[23] A. N. Mansour, " Characterization of β-Ni(OH) 2 by XPS ," *Surf. Sci. Spectra*, vol. 3, no. 3, pp. 239–246, Jul. 1994, doi: 10.1116/1.1247752.

[24] M. C. Biesinger, B. P. Payne, L. W. M. Lau, A. Gerson, and R. S. C. Smart, "X-ray photoelectron spectroscopic chemical state Quantification of mixed nickel metal, oxide and hydroxide systems," *Surf. Interface Anal.*, vol. 41, no. 4, pp. 324–332, 2009, doi: 10.1002/sia.3026.

[27] T. B. Daunis *et al.*, "Solution-processed oxide thin film transistors on shape memory polymer enabled by photochemical self-patterning," *J. Mater. Res.*, vol. 33, no. 17, pp. 2454–2462, 2018, doi: 10.1557/jmr.2018.296.